OPAL Physics Note PN-269
February 24, 1997

A Search for a Mass Peak in Four-Jet Events Produced in e^+e^- Collisions at $\sqrt{s} = 130 - 172$ GeV, Following the Selection of the ALEPH Collaboration

The OPAL Collaboration

Abstract

Events with four distinct jets, observed in e^+e^- collisions at centre-of-mass energies of 130–136, 161, and 170–172 GeV, are analysed for a peak in the sum of dijet masses. The selections and analyses described here follow closely those of the ALEPH collaboration, which observed an excess of events for dijet mass sums around 105 GeV. The estimated Standard Model background rates and detection efficiencies for a reference hA signal are nearly identical to those estimated by ALEPH. No mass peak near 105 GeV is observed by OPAL in data collected at any centre-of-mass energy.

This note describes preliminary OPAL results to be submitted to the XVIII International Symposium on Lepton-Photon Interactions, Hamburg, 28 July - 1 August 1997, and to the International Europhysics Conference on High Energy Physics, Jerusalem, 19-26 August 1997

1 Introduction

In the 130–136 GeV run of LEP, the ALEPH collaboration observed an excess of events with four distinct, fairly massive jets [1], compared to the Standard Model expectation. Grouping the jets into pairs, calculating their pair masses M_{ij} and M_{kl}, and selecting the combination yielding the minimum $\Delta M = |M_{ij} - M_{kl}|$, a clustering of nine events between 101.85$<M = M_{ij} + M_{kl} <$108.15 GeV was observed, with a Standard Model expectation of 0.8.

At the CERN seminar on the LEP 161 GeV run, ALEPH presented a preliminary search for the peak at 161 GeV energy [2] using essentially the same analysis, with the exceptions of taking into account energy dependence in some of the selection criteria and applying a requirement to reduce the W-pair background. At $\sqrt{s} = 161$ GeV, seven events were observed, with a Standard Model expectation of 7.2. Of these events, five had dijet mass sums of 100.5$< M <$110.1 GeV, with 1.0 expected from Standard Model backgrounds.

Recently ALEPH presented an update to the analysis with data collected near $\sqrt{s} =$ 172 GeV [3]. In the mass window mentioned above, ALEPH observed three events with a background expectation of 1.1. Summing contributions from all centre-of-mass energies, ALEPH has observed 18 events with dijet mass sums in the vicinity of 105 GeV with an expected background of 3.1 events.

Although the ALEPH analysis was originally designed to search for hA production, the observed cross-section disfavours this hypothesis. In addition, the properties of the events selected at 130-136 GeV were studied in detail and do not suggest hA production.

The ALEPH selection appears not to depend critically on the specific properties of the detector or data handling. OPAL emulated the ALEPH selection, searching for an excess of four-jet events in its 130-136 GeV data, and observed one event in the signal region indicated by ALEPH, in agreement with one expected background event [4]. DELPHI [5] and L3 [6] observed no peak at 105 GeV in similar analyses using their data at 130-136 GeV. Summing the event counts in DELPHI, L3, and OPAL, six events were observed, while 2.6 are expected from Standard Model background processes.

At 161 GeV, neither DELPHI [7] nor L3 [8] observed an excess of events using selections similar to ALEPH's and found in total three events with a background expectation of 3.3$\pm$0.9. OPAL has searched for hA production in the four-jet topology and has found no signal [9]. The estimated signal efficiency can be model dependent, as it is sensitive to the final state kinematics and particle content. In order to search for the same class of events observed by ALEPH in a model independent fashion, we have performed analyses on the OPAL data collected at $\sqrt{s}$ =130–136, 161, and 170–172 GeV as nearly identical as possible to the ALEPH analyses at these energies.

2 Analysis

The data used in these analyses were collected with the OPAL detector, which has been described in detail elsewhere [10], in three separate running periods. The energies and integrated luminosities for the three data samples are given in Table 1. The three samples are referred to in this note as the 133 GeV data (LEP 1.5), the 161 GeV data, and the 172 GeV data, and are analysed separately in order to follow the ALEPH analyses as closely as possible. The total integrated luminosity and the relative fractions accumulated in the different samples are similar between the two experiments.

$\sqrt{s}$ (GeV)	OPAL $\int\mathcal{L}dt$ (pb^{-1})	ALEPH $\int\mathcal{L}dt$ (pb^{-1})
130	2.6	2.8
136	2.6	2.8
161	10.0	11
170	1.0	1
172	9.2	7

Table 1: Summary of the data samples used in these analyses. Integrated luminosities taken by both OPAL and ALEPH are given separately for each centre-of-mass energy. The data taken at 130 and 136 GeV are combined in this note and referred to as the 133 GeV data. The second sample is referred to as the 161 GeV data, and the data taken at 170 and 172 GeV are combined and referred to as the 172 GeV data.

The tracking and calorimetry components used in the analyses are required to be fully operational for selected events. Good quality charged tracks are selected by requiring $|\cos\theta| <$ 0.98, where θ is the angle between the track and the beam axis, that the number of hits found in the central tracking detector is at least half of the expected number and at least 20, that the transverse momentum of the track is at least 100 MeV, that the total momentum of the track is not in excess of 100 GeV, that the track passes within 2.5 cm of the beam axis at a location along that axis not farther than 50 cm from the collision point, and that the chisquared of the track fit does not exceed 100 per degree of freedom either in $r-\phi$ or $s-z$ [1]. Calorimeter noise is suppressed by requiring electromagnetic calorimeter (ECAL) clusters to have at least one (two) contributing lead-glass blocks and energy of at least 100 (250) MeV in the barrel (endcap). Hadron calorimeter (HCAL) clusters are required to have at least 600 MeV in the barrel or endcap, and 2.0 GeV for the pole-tip hadron calorimeter. Tracks and clusters passing the quality requirements are then processed to reduce double-counting of energy and momentum in the event by matching charged tracks with calorimeter clusters. The energy-momentum flow obtained with this algorithm is used throughout the analysis. Details of the matching algorithm can be found elsewhere [11]. Energy measured in the forward detectors, covering $|\cos\theta| > 0.985$, has not been included in the analyses presented here.

The main backgrounds for these analyses are $Z^0/\gamma^* \to q\overline{q}$ production and four-fermion production processes. The main component of the latter comes from W^+W^- production for centre-of-mass energies above the kinematic threshold for this process. Monte Carlo samples modelling

[1] In OPAL, the electron beam travels along the z axis. The $r-\phi$ plane is perpendicular to the z axis. The coordinate s denotes arc length along a track.

the backgrounds have been prepared using PYTHIA 5.7 [12] for the $Z^0/\gamma^* \rightarrow q\overline{q}$ process with fragmentation and hadronisation using JETSET 7.4 [12], and EXCALIBUR [13] and grc4f [14] for the four-fermion processes, both using JETSET 7.4's parton shower and hadronization models. For the generation of four-fermion processes, the W mass is taken to be 80.33 GeV. The size of the samples exceeds 100 times the collected luminosity. Two-photon processes generated by PYTHIA, HERWIG [15], and PHOJET [16] were used to estimate the contribution of these processes to the Standard Model background in the early stages of the analysis. All Monte Carlo samples were processed through a full simulation of the OPAL detector [17].

The procedure for selecting four-jet hadronic events and reconstructing the dijet masses is described below, following the ALEPH procedure [1] in detail. The number of events retained after each cut in sequence is given in Tables 2, 3, and 4, together with the expectation from $Z^0/\gamma^* \rightarrow q\overline{q}$, four-fermion, and two-photon background processes, for the different centre-of-mass energies. Backgrounds from lepton pair production are not included in the tables since they are found to be negligible after the multi-hadron selection.

1. Hadronic Final State: Events are required to have at least five charged tracks and seven electromagnetic calorimeter clusters. The sum of the ECAL cluster energies should be at least 10% of the centre-of-mass energy, and the ECAL energy is required to be roughly balanced along the beam direction: $\sum E_i \cos\theta_i \leq 0.65 \sum E_i$, where the sums run over measured ECAL clusters. The properties of this selection are detailed in Reference [18].

   For comparison, the ALEPH hadronic event selection requires at least eight charged tracks, and the sum of the charged particle momenta must exceed 10% of the centre-of-mass energy.

2. Radiative return rejection: to remove events with a real Z^0 and large initial state radiation, events must satisfy $|p_z^{vis}| \leq C(M_{vis} - 90)$ (GeV), where p_z^{vis} is the momentum sum along the beam direction and $M_{vis} = \sqrt{E_{vis}^2 - p_{vis}^2}$ is the total observed mass. C is a coefficient depending on $\sqrt{s}$. For the 130–136 GeV sample, $C = 0.75$, for the 161 GeV sample, $C = 1.50$, and for the 170–172 GeV sample, $C = 1.65$.

3. Four-jet final state: Jets are formed with the Durham jet-finding algorithm [19] with its resolution parameter y_{cut} set to 0.008. Selected events are required to have four or more such jets. For events with five jets, the jet pair with the smallest invariant mass is combined into a single jet. In no event were six jets formed, consistent with the expectation from simulation.

4. Rejection of events with γ-like jets: The ALEPH analysis requires that none of the four jets contains more than 80% electromagnetic energy in order to reduce further the contribution from radiative return events. This has been emulated by requiring for each jet that the energy observed in the ECAL, after subtracting the expected energy deposited by charged hadrons using the matching algorithm, should be less than 80% of the jet energy for each jet.

5. Large individual jet masses: All jet masses are required to exceed 1.0 GeV to suppress further the contribution from radiative returns.

6. Jet energy scaling: The energies and momenta of each jet are rescaled imposing conservation of energy and momentum for the event using the beam energy constraint. The jet velocities $\vec{\beta}_i = \vec{p}_i/E_i$ are held fixed in the scaling. If one or more scaling factors is negative, the event is rejected. The rescaled jet energies and momenta are used in the following stages of the selection.

7. Large dijet masses: To suppress events involving gluon radiation, all two-jet combinations are required to have an invariant mass of more than 19.2% of the centre-of-mass energy. This corresponds to 25 GeV for the 133 GeV sample, 31 GeV for the 161 GeV sample, and 33 GeV for the 172 GeV sample.

8. Large pairwise sums of jet masses: All combinations of jet pairs must have a sum of the individual jet masses $M_i + M_j > 10$ GeV.

9. High multiplicity of jet pairs: All combinations of two jets must have a total charged multiplicity of at least 10.

10. W-pair veto: For the 161 GeV data sample, a requirement is placed on the dijet mass sum for each of the three possible pairings of jets: $M \leq 150$ GeV for the pairing with the smallest ΔM, $M \leq 152$ GeV for the pairing with intermediate ΔM, and $M \leq 156$ GeV for the pairing with the largest ΔM. For the 172 GeV data, the following two conditions are demanded: $|M - 160| \geq 10$ GeV for the smallest ΔM if the mass difference is less than 15 GeV, and $|M - 160| \geq 10$ GeV for the intermediate ΔM if the mass difference is less than 30 GeV. No W-pair veto is applied to the 133 GeV sample.

Table 2, which summarises the selection at 133 GeV, shows agreement between the background expectation and observation, while that for the 161 GeV data, Table 3, shows an excess in the total number of events observed in data compared with the Monte Carlo expectation after the four-jet requirement and especially before the final W-pair veto. The 172 GeV data shows a discrepancy with the Standard Model expectation only in the early stages of the selection, indicating that poorly modelled events do not resemble those sought by this analysis.

The sum of the dijet masses, M, for the combination with the smallest dijet mass difference, ΔM, is shown separately for the three data samples in Figures 1, 2, and 3, for each stage of the selection between cuts (6) and (10). The expected Standard Model background distribution is shown with the data for each case.

The dijet mass sums retained after cut (6) for the 130–136 GeV sample and after cut (9) for higher energy are listed in Tables 15, 16, and 17. In these tables, "*" indicates the event passes all selection requirements.

To search for an excess of four-jet events with dijet mass sums near 105 GeV, events satisfying $|M - 105 \text{ GeV}| < 2\sigma$ for the combination with the smallest ΔM were counted and the Standard Model backgrounds were estimated. The expected resolution on M, denoted by σ, is expected to depend on $\sqrt{s}$, and this dependence is given in Table 6. The results of the searches within these mass regions are shown in Table 5 both before and after the W-pair veto, when applicable. No significant excess is seen for any sample.

Cut	$Z^0/\gamma^* \to q\overline{q}$	4-Fermion	$\gamma\gamma$	Total Standard Model	Data
(1)	1466.7	10.8	74.2	1551.7±8.2	1537
(2)	549.2	7.1	4.1	560.5±4.1	527
(3)	70.3	1.8	0.8	72.9±1.5	73
(4)	27.3	1.6	0.8	29.7±1.1	24
(5)	24.4	1.4	0.8	26.6±1.0	21
(6)	21.3	1.3	0.8	23.4±1.0	19
(7)	10.3	0.7	0.5	11.5±0.7	10
(8)	8.7	0.5	0.0	9.2±0.5	10
(9)	6.8	0.3	0.0	7.1±0.4	8

Table 2: 133 GeV: Event counts observed by OPAL at the various selection stages, with backgrounds estimated using PYTHIA for $Z^0/\gamma^* \to q\overline{q}$, EXCALIBUR for four-fermion processes, and PYTHIA and PHOJET for two-photon processes. The errors shown arise from limited Monte Carlo statistics.

Cut	$Z^0/\gamma^* \to q\overline{q}$	4-Fermion	$\gamma\gamma$	Total Standard Model	Data
(1)	1345.9	52.5	45.5	1443.9±3.5	1499
(2)	573.1	40.9	0.9	614.9±2.3	648
(3)	57.3	17.9	0.0	75.2±0.8	92
(4)	22.1	16.0	0.0	38.1±0.6	51
(5)	20.6	14.7	0.0	35.3±0.5	49
(6)	18.3	12.9	0.0	31.2±0.5	39
(7)	7.8	9.3	0.0	17.1±0.4	22
(8)	6.9	8.2	0.0	15.1±0.4	22
(9)	5.6	6.4	0.0	12.0±0.3	18
(10)	4.1	2.1	0.0	6.2±0.2	7

Table 3: 161 GeV: Event counts observed by OPAL at the various selection stages, with backgrounds estimated using PYTHIA for $Z^0/\gamma^* \to q\overline{q}$, EXCALIBUR for four-fermion processes, and PYTHIA and PHOJET for two-photon processes. The four-fermion cross-section is calculated taking the W mass to be 80.33 GeV. The errors shown arise from limited Monte Carlo statistics.

Cut	$Z^0/\gamma^* \to q\overline{q}$	4-Fermion	$\gamma\gamma$	Total Standard Model	Data
(1)	1109.2	125.7	31.8	1266.6±3.6	1404
(2)	488.1	103.7	0.6	592.4±1.8	596
(3)	50.9	56.4	0.0	107.3±0.7	116
(4)	22.8	51.7	0.0	74.5±0.5	78
(5)	20.3	48.6	0.0	68.9±0.5	73
(6)	16.3	43.5	0.0	59.8±0.4	63
(7)	6.7	32.4	0.0	39.1±0.3	41
(8)	6.1	30.2	0.0	36.2±0.3	36
(9)	5.0	24.5	0.0	29.4±0.3	26
(10)	3.7	9.1	0.0	12.7±0.2	5

Table 4: 172 GeV: Event counts observed by OPAL at the various selection stages with backgrounds estimated using PYTHIA for $Z^0/\gamma^* \to q\overline{q}$, grc4f for four-fermion processes, and PYTHIA and HERWIG for two-photon processes. The errors shown arise from limited Monte Carlo statistics.

	Without W-Pair Veto		With W-Pair Veto	
Data Sample	Observed	Background	Observed	Background
133 GeV	1	1.0	—	—
161 GeV	1	1.5	0	1.0
172 GeV	3	2.9	0	1.7

Table 5: Observed event count and estimated Standard Model background for selected events close to 105 GeV, for the combination with the smallest ΔM, before and after the W-pair veto, where applicable. The mass window is chosen to allow events that are within $\pm 2\sigma$ of 105 GeV to be included, where σ is the expected experimental resolution on M, whose dependence on $\sqrt{s}$ is given in Table 6.

3 Selection Performance Comparison

To evaluate the quality of the emulation, and also to ensure that detector differences do not affect the performance of the analysis, we compare both the estimated signal efficiency for hA production and the estimated Standard Model background rates with those quoted by ALEPH [1].

3.1 hA Signal Detection Efficiency

The process $e^+e^- \rightarrow$hA was modelled with the HZHA event generator [20]. For comparison with ALEPH's estimated efficiencies, the masses of both h and A are taken to be equal to 55 GeV with negligible width. The resolutions for the reconstructed dijet mass sum M for the combination with the smallest ΔM for the ALEPH and OPAL analyses at the three centre-of-mass energies are listed in Table 6. The distribution of M for this combination for the simulated hA signal generated with $\sqrt{s} = 161$ GeV is shown in Figure 4, together with that for the corresponding ΔM. The non-Gaussian tails come from wrong jet-pair combinations and are not included in the resolutions listed in Table 6. This definition of the resolution is the same as that used in the ALEPH analyses [1]. The degradation of mass resolution with increasing energy arises from the scaling of the jet energies to the beam energy and also from the energy dependence of the detector resolution.

Data Sample	OPAL σ_M (GeV)	ALEPH σ_M (GeV)
133 GeV	2.0	1.6
161 GeV	2.8	2.4
172 GeV	3.0	$\sim$2.4

Table 6: Resolution of the dijet mass sum M for the combination with the smallest ΔM for the ALEPH and OPAL analyses for the different data samples. ALEPH reports a "similar" resolution at 172 GeV to that estimated at 161 GeV.

For signal samples generated at each centre-of-mass energy, the locations of peaks in the distributions of M are consistent with 110 GeV, expected from the masses input to the generator, within their errors of $\sim$0.5 GeV. ALEPH also estimates no bias in M within an accuracy of 1 GeV [1].

The efficiencies for the reference signal Monte Carlo are shown in Table 7 for the 133 GeV analysis after each step of the selection. The OPAL and ALEPH analyses perform very similarly after each step. If the reconstructed dijet mass sum for the jet-pair combination having the smallest ΔM is required to be within 2.0σ (4.0 GeV) of the generated mass sum, the efficiency obtained is 26.6%, which corresponds to 60% of the efficiency obtained without the requirement on M. This loss of efficiency from the mass window requirement is consistent with ALEPH's estimation of 60%. The behaviour of the signal selection efficiency of this analysis is therefore believed to be similar to that of the ALEPH analysis for the minimum ΔM combination both before and after a $\pm 2\sigma$ mass window requirement.

Cut	ϵ_{hA} OPAL	ϵ_{hA} ALEPH	Bkg OPAL	Bkg ALEPH
(1)	99.8	99.8	1551.7	1669.5
(2)	90.2	92.4	560.5	723.4
(3)	69.0	69.8	72.9	128.6
(4)	67.4	—	29.7	—
(5)	67.2	67.8	26.6	29.6
(6)	65.4	65.6	23.4	27.5
(7)	49.6	55.0	11.5	14.9
(8)	48.6	48.6	9.2	10.7
(9)	45.4	42.0	7.1	7.8

Table 7: Comparison of the efficiencies of the OPAL and ALEPH 133 GeV analyses for the reference (55+55 GeV) hA signal and expected Standard Model background for each step of the selection. The background expectation for the ALEPH analysis, quoted originally for an integrated luminosity of 5.7 pb^{-1}, has been scaled to the luminosity taken by OPAL, 5.2 pb^{-1}.

The estimated efficiencies of the OPAL and ALEPH analyses at 161 GeV, shown in Table 8, are similar with and without the W-pair veto, and also with and without a mass window requirement. Before applying the W-pair veto, the efficiency for hA production is estimated to be 40.6% (ALEPH obtains 40%). After applying the W-pair veto, this analysis obtains 27.9% (ALEPH obtains 30%). Accepting events only in the mass window of $\pm$5.6 GeV, corresponding to $\pm 2\sigma$, reduces both efficiencies by roughly a factor of 0.7: the efficiency without the W-pair veto decreases to 26.2%, and the efficiency with the W-pair veto to 18.4%. A decrease in efficiency by a factor of 0.7 is also estimated by ALEPH when a mass window of $\pm 2\sigma$ is applied. Detailed estimates of the signal efficiency of the ALEPH analysis at 172 GeV are not yet available.

While hA production is disfavoured as an explanation for ALEPH's excess events [1], testing the OPAL and ALEPH selections with the same simulated signal and achieving similar efficiencies lends confidence that the emulated analyses share the sensitivity of the ALEPH analyses to new signals, provided that they are similar to the hA signal. If the excess events observed by ALEPH tend to have one or more jets very close to the beam pipe, the analyses here might

		OPAL	ALEPH
Without W-pair veto	hA efficiency	40.6%	40%
	SM background	12.0	12.5
With W-pair veto	hA efficiency	27.9%	30%
	SM background	6.2	6.5

Table 8: Performance comparison between the OPAL emulation and the ALEPH analysis for 161 GeV. Signal efficiencies apply to hA production with $M_A = M_h = 55$ GeV. The Standard Model (SM) background estimations for both the ALEPH and OPAL analyses have been normalized to the same integrated luminosity of 10 pb^{-1} taken by OPAL.

have different efficiencies from ALEPH's due to the omission of the forward detector energy. The properties of the events reported by ALEPH do not indicate that this is the case, though, and the efficiency for well-contained events is expected to be similar.

3.2 Standard Model Background Rate

The estimations of the Standard Model backgrounds in the emulated analyses listed in Tables 2, 3, and 4 agree with those estimated by ALEPH, after all selection requirements have been applied. Table 7 shows the expected background for the OPAL and ALEPH 133 GeV analyses after each step of the selection. The expected background levels are normalized to the same integrated luminosity, 5.2 pb^{-1}, taken by OPAL. There are discrepancies from cuts (1) to (3), which may be expected from the fact that information from the OPAL forward detector is omitted in the energy flow calculation, while ALEPH's angular acceptance includes the forward region. The effect of this is to modify the estimated contamination from radiative return events from cuts (1) to (3). After further suppression of these events in cuts (4) and (5), the two analyses show reasonable agreement. An estimated 7.1 ± 0.4 events from Standard Model processes are expected to pass all selection requirements in the OPAL emulated analysis, while ALEPH estimates 7.8.

For the 161 and 172 GeV data, information from ALEPH is only available after the final analysis cut and the W-pair veto. For the 161 GeV analysis, the estimated background in the emulated analysis is 12.0 ± 0.3 (6.2 ± 0.2) events, while ALEPH estimates 12.5 (6.5), normalized to OPAL's 10.0 pb^{-1}, before (after) the W-pair veto. For the 172 GeV analysis, the estimated background in the emulated analysis is 29.4 ± 0.3 (12.7 ± 0.2) events, while ALEPH estimates 26.4 (12.1) events, normalized to OPAL's 10.2 pb^{-1}, before (after) the W-pair veto.

We believe we have successfully emulated the ALEPH four-jet selections and analyses because the estimated signal detection efficiencies, mass resolutions, and backgrounds from Standard Model processes are similar in all details. The sensitivity to new physics and the likelihood of a background fluctuation are nearly identical between the original ALEPH analyses and the OPAL emulations presented here.

4 Studies with Looser Selections

In the above analyses the ALEPH selection criteria were used with OPAL data, although the performance of the OPAL detector is not identical to that of ALEPH. For example, the total visible energy resolution for the multihadronic Z^0 decays observed at LEP1 is somewhat poorer with OPAL than with ALEPH, potentially affecting the selection efficiency. Also the charged multiplicity depends on the track quality definition. To ensure that a possible signal has not been missed due to an inappropriately conservative selection, the search has been repeated with the OPAL 161 GeV data sample loosening requirements (7) to (9), scaling the selection values down by 20%. The W-pair veto also depends on the mass resolution, hence results are presented both before and after the W-pair veto.

A comparison of the looser selection with the original analysis is shown in Table 9 for the OPAL 161 GeV data. These variations do not change significantly the number of observed events in the region 99.4$< M <$110.6 GeV, and the number of observed events remains consistent with the expected number of background events. Figure 5 shows the distribution of the dijet mass sum for the combination with the smallest ΔM for the analysis loosening requirements (7) to (9) for all three data samples. The W-pair veto has not been applied in the figure. Table 10 lists the event counts in the signal region for each data sample. No excess is observed in the vicinity of M=105 GeV in any sample, and none appears when the intermediate ΔM combination is added.

Because cut (4) depends on the detector configuration, especially the granularity of the ECAL, a test was made omitting it from the analysis. With this selection, nine events are observed with a background expectation of 7.2 events in the 161 GeV data sample. No events are found in the mass window $\pm$5.6 GeV centred at 105 GeV.

If OPAL's energy measurement calibration differs from that of ALEPH, or if the mass of the signal events differs from the reported value, then the signal may appear outside the recommended search region. Excesses of events were sought in the 161 GeV data with dijet mass sums between 100 to 110 GeV by displacing the center of the mass window, of width 11.2 GeV, in small steps. Before applying the W-pair veto, the observed number of events never exceeds three, consistent with a constant expectation of 1.5 events. Once the W-pair veto is applied, no more than one event remains in any mass window centred between 100 to 110 GeV. No significant excess beyond 1σ of the statistical uncertainty is observed in the OPAL 161 GeV data for any dijet mass sum between 100 to 110 GeV.

5 Mass Distributions for Other Jet Pairings

The distributions of M for the other two combinations of the jet pairing, i.e. the intermediate and largest ΔM, have been analysed for evidence of a signal. If the mass difference of a pair of objects produced together were 20 GeV, the correct jet pairing would yield the smallest ΔM for roughly half of the signal, and the intermediate ΔM for most of the remainder. Figures 6–10 show the dijet mass sums adding to the smallest-ΔM distribution contributions from the

			No Mass Window		With Mass Window	
Cut	Original	Loose	Expect	Data	Expect	Data
Cuts (1–9)			11.6	18	1.5	1
(7a)	31 GeV	25 GeV	16.2	25	2.0	3
(8a)	10 GeV	8 GeV	12.0	18	1.6	1
(9a)	10	8	13.4	20	1.7	1
(a)			20.6	27	2.4	3
Cuts (1–10)			6.1	7	1.0	0
(7b)	31 GeV	25 GeV	9.6	13	1.5	2
(8b)	10 GeV	8 GeV	6.3	7	1.0	0
(9b)	10	8	7.1	7	1.1	0
(b)			12.3	13	1.8	2

Table 9: The number of expected and observed events at $\sqrt{s} = 161$ GeV with looser selection values for cuts (7), (8) and (9). Line 7a: cut (7) is loosened to 25 GeV from its original 31 GeV, holding the other cuts constant; Line 8a: similar to Line 7a but only cut (8) is loosened; Line 9a: only cut (9) is loosened. Lines 7a, 8a, and 9a correspond to selections without the W-pair veto, while lines 7b, 8b, and 9b are analogous loosenings of the requirements with the W-pair veto applied. Lines a and b show the effect of loosening cuts (7), (8) and (9) simultaneously. The events in the rightmost two columns must satisfy a mass window requirement of $99.4 < M < 110.6$ GeV for the combination with the smallest ΔM.

		No Mass Window		With Mass Window	
Sample	Mass Window (GeV)	Expect	Data	Expect	Data
133 GeV	101.0–109.0	14.55	13	1.9	1
161 GeV	99.4–110.6	12.3	13	1.8	2
172 GeV	99.0–111.0	46.1	57	4.3	6

Table 10: Looser selections performed on the three data samples separately. Shown are the numbers of expected and observed events in selections relaxing cuts (7)–(9) by 20%. The listed mass window requirement has been applied to the combination with the smallest ΔM, but the W-pair veto has not been applied.

intermediate and largest ΔM jet-pair combinations, for analyses before and after W-pair veto. None of the distributions shows a significant peak, particularly near 105 GeV.

6 Combined Results for All Energies

The selected events are combined below for the data samples collected at the three centre-of-mass energies. The total number of events observed and expected from Standard Model processes is presented in Table 11, for all stages of the selection. Figure 11 shows the distribution of the dijet mass sum for the different jet pairings combined for all running periods, without the W-pair veto, and Figure 12 shows the same distributions after the W-pair veto has been applied. The data agree well with the Standard Model background simulation and no excess is observed in the region 99.4< M <110.6 GeV.

cut	Observed Events	Total Standard Model
(1)	4440	4262.2±9.6
(2)	1771	1767.8±5.0
(3)	281	255.4±1.8
(4)	153	142.3±1.3
(5)	143	130.8±1.2
(6)	121	114.4±1.2
(7)	73	67.7± .9
(8)	68	60.5± .7
(9)	52	48.5± .6
(10)	20	26.0± .5

Table 11: Observed event counts and expected Standard Model backgrounds after each stage of the selection, summed for the three data samples, details of which are given in Tables 2, 3, and 4.

To perform a more general search for local excesses of four-jet events, sliding mass window scans, which show the event counts within windows of fixed width but whose centers are adjusted in steps of 50 MeV, are shown in Figures 13 and 14. The width of the mass window is ±4.0, ±5.6, and ±6.0 GeV for the 133, 161 and 172 GeV data samples, respectively, to reflect the resolution, and the results are combined for the three data samples in each of the scans. Figure 13 shows the scan for events after cut (9), i.e. before the W-pair veto for 161 and 172 GeV, and Figure 14 shows the scan for events passing all selections requirements. The scans were performed for the smallest ΔM combination alone, the combination of the smallest and intermediate ΔM, and also for all three combinations. The contents of nearby bins in these scans have high statistical correlations. No significant excess is observed in any of the sliding mass window scans at any value of the dijet mass sum.

7 Upper Limits on Observed Event Averages

The 95% confidence-level upper limit on the average number of events expected to be observed in the mass window has been calculated using the OPAL data both with and without subtraction of the expected background, and the results are shown in Table 12, compared with the ALEPH observations. To calculate the limit with background subtraction, the conservative PDG [21] procedure has been adopted. In each case, the limit reported has been scaled to the integrated luminosity of the ALEPH combined analyses, 24.7 pb^{-1}, from the OPAL combined luminosity of 25.4 pb^{-1}. The contributions to the OPAL and ALEPH integrated luminosities from the data samples of different centre-of-mass energy are very similar, hence the comparison of the OPAL limits on the total number of events with the ALEPH observations depends very little on the energy dependence of the four-jet production cross-section.

The width of the mass window for each energy is scaled with the expected signal resolution; the widths are ± 4.0 GeV, ± 5.6 GeV, and ± 6.0 GeV for the 133, 161, and 172 GeV data samples, respectively. In calculating the limits including background subtraction, the background levels have been estimated by scaling the simulated Standard Model background to the observed number of selected events outside of the mass windows.

To ensure that signal has not been lost due to a difference in detector energy scales, the upper limits are also calculated in each case for the mass window centered between 102 and 108 GeV which provides the most conservative upper limit on the event count average. The limits are also shown combining the smallest and intermediate jet pairings as well as all three jet pairings, in Tables 13 and 14.

A probability of consistency between the raw ALEPH and OPAL event counts may be formed, as the analyses and data samples are similar. The joint probability P of observing at least N_{ALEPH} in ALEPH within the mass window and no more than N_{OPAL} events in OPAL in a similar mass window has been calculated using [2]

$$P = \left(\sum_{i=0}^{N_{\mathrm{OPAL}}} \frac{\mu^i e^{-\mu}}{i!} \right) \left(\sum_{i=N_{\mathrm{ALEPH}}}^{\infty} \frac{\mu^i e^{-\mu}}{i!} \right) \tag{1}$$

with an arbitrary mean μ. This mean is then varied to maximise P. As given in Table 12 for the case without the W-pair veto, N_{ALEPH}=19 and N_{OPAL}=5. The Poisson distribution most consistent with both of these observations has a mean of 12.38 and the probability of observing these event counts is 7.7×10^{-4}. After the W-pair veto, N_{ALEPH}=18 and N_{OPAL}=1. The mean then becomes 9.92 and the probability falls to 7.1×10^{-6}. The optimal mean must be recalculated when incorporating the observations of the other LEP experiments. It should also be noted that these probabilities have been calculated for the most discrepant part of a histogram with many bins and hence are biased towards low probabilities.

[2] Minor corrections have been made since the first draft. Equation 1 now contains the correct Poisson probability formula, and the probabilities have been corrected.

	Fixed Mass Window		Conservative Mass Window	
	No W-Veto	W-Veto	No W-Veto	W-Veto
Observed Events	5	1	6	2
Expected Background	5.6	3.1	5.4	2.8
95% CL Limit No Bg Subt.	10.2	4.6	11.9	6.3
95% CL Limit Bg Subt.	5.9	3.5	7.1	4.5
ALEPH Data	19	18	—	—
ALEPH Expected Bg	4.3	3.2	—	—

Table 12: Calculation of the 95% confidence-level upper limit on the average number of events passing the selections for all energies combined. The limits are shown for events falling in mass windows centered at M=105 GeV of width $\pm$4.0, $\pm$5.6, and $\pm$6.0 GeV for the 133, 161, and 172 GeV data samples, respectively. The limits are also calculated choosing the centers of the mass windows within the interval 102 to 108 GeV that produce the largest upper limit. Only the jet-pairing combination with the smallest ΔM is used in the calculation. In each case, the limits have been scaled to the ALEPH integrated luminosity.

	Fixed Mass Window		Conservative Mass Window	
	No W-Veto	W-Veto	No W-Veto	W-Veto
Observed Events	7	2	10	4
Expected Background	12.4	5.7	10.1	4.6
95% CL Limit No Bg Subt.	12.8	6.1	16.5	8.9
95% CL Limit Bg Subt.	5.1	3.7	7.8	5.5

Table 13: Calculation of the 95% confidence-level upper limit on the average number of events passing the selections for all energies combined. The limits are as in Table 12, but the event counts have been accumulated for the smallest and intermediate ΔM jet pairings.

	Fixed Mass Window		Conservative Mass Window	
	No W-Veto	W-Veto	No W-Veto	W-Veto
Observed Events	12	2	14	4
Expected Background	13.6	6.6	11.4	7.8
95% CL Limit No Bg Subt.	18.9	6.1	21.3	8.9
95% CL Limit Bg Subt.	7.6	3.7	10.7	4.5

Table 14: Calculation of the 95% confidence-level upper limit on the average number of events passing the selections for all energies combined. The limits are as in Table 12, but the event counts have been accumulated for all three possible jet pairings.

8 Conclusions

A careful emulation of the ALEPH analysis has been performed with OPAL's sample of 5.2 pb^{-1} of e^+e^- collisions at $\sqrt{s} \sim 133$ GeV, 10.0 pb^{-1} at $\sqrt{s} \sim 161$ GeV and 10.2 pb^{-1} at 172 GeV. The estimated sensitivity of this analysis to hA production is nearly identical to that of the ALEPH analysis, independent of differences in detector performance and data handling, and the mass resolutions are similar. The estimated Standard Model backgrounds are also nearly identical between the two analyses. No significant excess of four-jet events with dijet mass sums in the region close to 105 GeV, or any other region between 60 and 160 GeV, has been observed in any of the data samples separately or combined, and no excess appears when the selection requirements are significantly loosened.

References

[1] D. Buskulic *et al.,* ALEPH Collaboration, *Z. Phys.* C **71**, 179 (1996).

[2] R. Miquel, for the ALEPH Collaboration; presentation at the CERN LEPC seminar on 8 October, 1996.

[3] F. Ragusa, for the ALEPH Collaboration; presentation at the CERN LEPC seminar on 19 November, 1996.

[4] OPAL Collaboration, G. Alexander *et al.,* CERN-PPE 96-096.

[5] DELPHI Collaboration, P. Abreu *et al.,* CERN-PPE 96-119.

[6] L3 Collaboration, *Study of Events with two Lepton plus Jets or with four Jets in* e^+e^- *Collisions at Center of Mass Energies between 130 and 140 GeV*, pa13-018, Contribution to Warsaw.

[7] W. deBoer, for the DELPHI Collaboration; presentation at the CERN seminar on Oct 8, 1996.

[8] M. Pohl, for the L3 Collaboration; presentation at the CERN seminar on Oct 8, 1996.

[9] OPAL Collaboration, Physics note PN260.

[10] OPAL Collaboration, K. Ahmet *et al.,* , *Nucl. Instrum. Methods* A305 (1991) 275; P.P. Allport *et al.,* , *Nucl. Instrum. Methods* A324 (1993) 34; P.P. Allport *et al.,* , *Nucl. Instrum. Methods* A346 (1994) 476.

[11] OPAL Collaboration, K. Ackerstaff *et al.,* CERN-PPE 96-135. (accepted by Phys. Lett.)

[12] PYTHIA 5.721 and JETSET 7.408 generators: T. Sjöstrand, Comp. Phys. Comm. 82 (1994) 74; T. Sjöstrand, LUTP 95-20.

[13] EXCALIBUR generator: F.A. Berends, R. Pittau, R. Kleiss, Comp. Phys. 85 (1995) 437.

[14] J. Fujimoto *et al.,* KEK-CP-046 (unpublished).
Minami-Tateya collaboration, “GRACE manual ver. 1.0”, KEK Report **92-19**, 1993,
Minami-Tateya collaboration, “Brief Manual of GRACE system ver 2.0/β”, 1995.

[15] HERWIG generator: G. Marchesini *et al.,* Comp. Phys. Comm. 67 (1992) 465.

[16] R. Engel, in *Physics at LEP2*, eds. G. Altarelli, T. Sjöstrand and F. Zwirner, CERN 96-01, vol. 2, p. 216 (1996).

[17] J. Allison *et al.,* Nucl. Instr. and Meth. **A317** (1992) 47.

[18] OPAL Collaboration, G. Alexander *et al.,* Z. Phys. **C52** (1991) 175.

[19] N. Brown and W.J. Stirling, *Phys. Lett.* B252 (1990) 657;
S. Bethke, Z. Kunszt, D. Soper and W.J. Stirling, *Nucl. Phys.* B370 (1992) 310;
S. Catani *et al.,* , *Phys. Lett.* B269 (1991) 432;
N. Brown and W.J. Stirling, *Z. Phys.* C53 (1992) 629.

[20] HZHA generator: P. Janot, in Physics at LEP2, edited by G. Altarelli, T. Sjöstrand and F. Zwirner, CERN 96-01, vol.2 (1996) p.309.

[21] Particle Data Group, *Phys. Rev.* **D50** (1994) 1281-1282.

	SmallestΔM	Intermediate ΔM	Largest ΔM
	107.2	102.0	94.9
	127.4	124.6	53.9
*	86.4	98.1	127.5
	85.3	128.7	106.0
*	125.8	110.7	81.8
*	107.0	87.1	128.0
	122.0	54.4	130.0
*	57.7	115.3	123.1
	116.7	81.1	111.1
	88.1	92.7	121.6
	92.0	92.4	127.8
*	97.2	104.0	132.1
*	87.8	121.4	120.2
	134.5	127.9	69.7
	106.3	106.0	95.8
*	129.1	75.0	124.3
	98.8	90.7	117.4
*	83.6	125.5	122.3
	117.9	98.8	101.4

Table 15: 133 GeV: The sum of dijet masses, M (GeV), for the selected events after cut (6). Listed are the values for the jet associations giving the smallest, intermediate, and largest ΔM. Events passing all nine selection requirements used at 133 GeV are indicated with a "*". The expected resolution in M at this energy is 2.0 GeV.

	SmallestΔM	Intermediate ΔM	Largest ΔM
	156.8	91.1	150.9
*	98.0	146.4	125.3
*	117.5	151.6	123.8
	82.7	155.1	148.6
	99.8	159.8	139.1
*	96.9	130.3	156.0
	141.5	156.9	110.3
*	142.4	91.5	139.5
	138.6	154.5	94.9
	141.6	157.9	107.0
	130.3	152.1	108.4
	156.1	140.0	94.8
	149.3	77.4	160.1
*	117.2	130.1	137.8
*	113.4	138.6	131.3
	158.0	130.0	107.0
	124.0	97.0	158.1
*	142.0	86.9	142.6

Table 16: 161 GeV: The sum of dijet masses, M (GeV), for the selected events after cut (9). Listed are the values for the jet associations giving the smallest, intermediate, and largest ΔM. Events passing all ten selection requirements are indicated with a "*". The expected resolution in M at this energy is 2.8 GeV.

	SmallestΔM	Intermediate ΔM	Largest ΔM
*	124.4	146.4	152.4
	155.2	135.2	137.9
	156.2	161.0	99.2
	155.3	122.8	137.9
*	122.8	142.9	145.2
	126.9	156.1	142.4
	157.4	82.9	167.0
	159.3	157.1	97.4
*	133.2	119.7	140.7
	109.6	154.7	140.2
*	123.6	159.1	125.0
	161.2	118.6	144.3
	142.8	164.5	132.4
	120.4	161.3	143.8
	158.2	103.4	157.7
	115.9	163.4	140.2
	156.1	154.6	122.4
	90.4	164.8	162.5
	86.0	158.6	158.9
	112.9	162.3	148.0
	150.3	115.7	161.1
*	135.8	143.4	161.1
	96.7	150.8	167.0
	104.3	158.4	156.9
	92.7	157.7	162.0
	105.6	153.0	152.4

Table 17: 172 GeV: The sum of dijet masses, M (GeV), for the selected events after cut (9). Listed are the values for the jet associations giving the smallest, intermediate and largest ΔM. Events passing all ten selection requirements are indicated with a "*". The expected resolutions in M at this energy is 3.0 GeV.

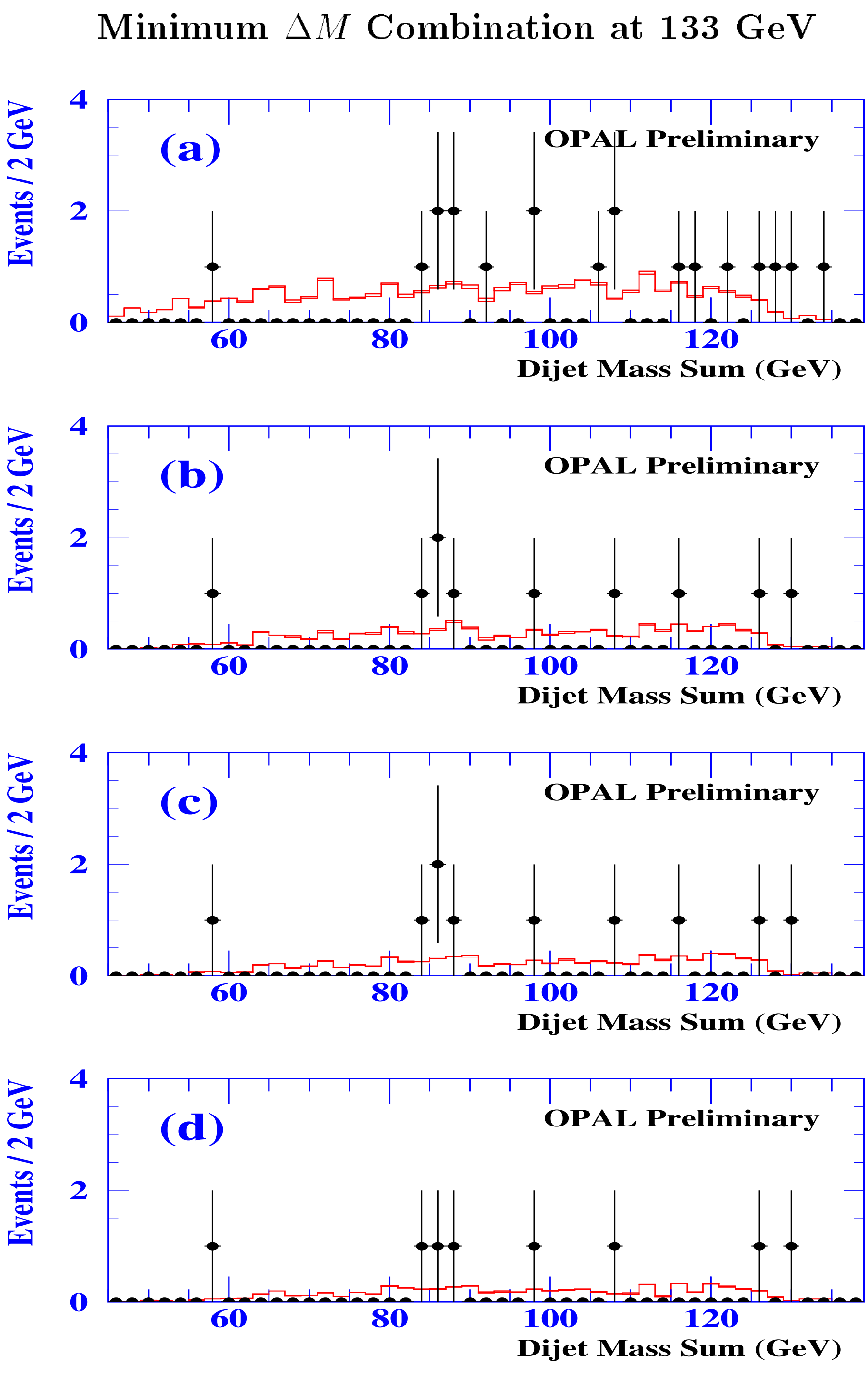

Figure 1: 133 GeV: The dijet mass sum for the combination with the smallest ΔM at different stages of the selection. Plots (a)–(d) show the distribution after cuts (6)–(9), respectively. Data are shown by points and Standard Model backgrounds by the histogram. The hatched component of the background histogram denotes four-fermion processes, while the unhatched component denotes $Z^0/\gamma^* \to q\overline{q}$.

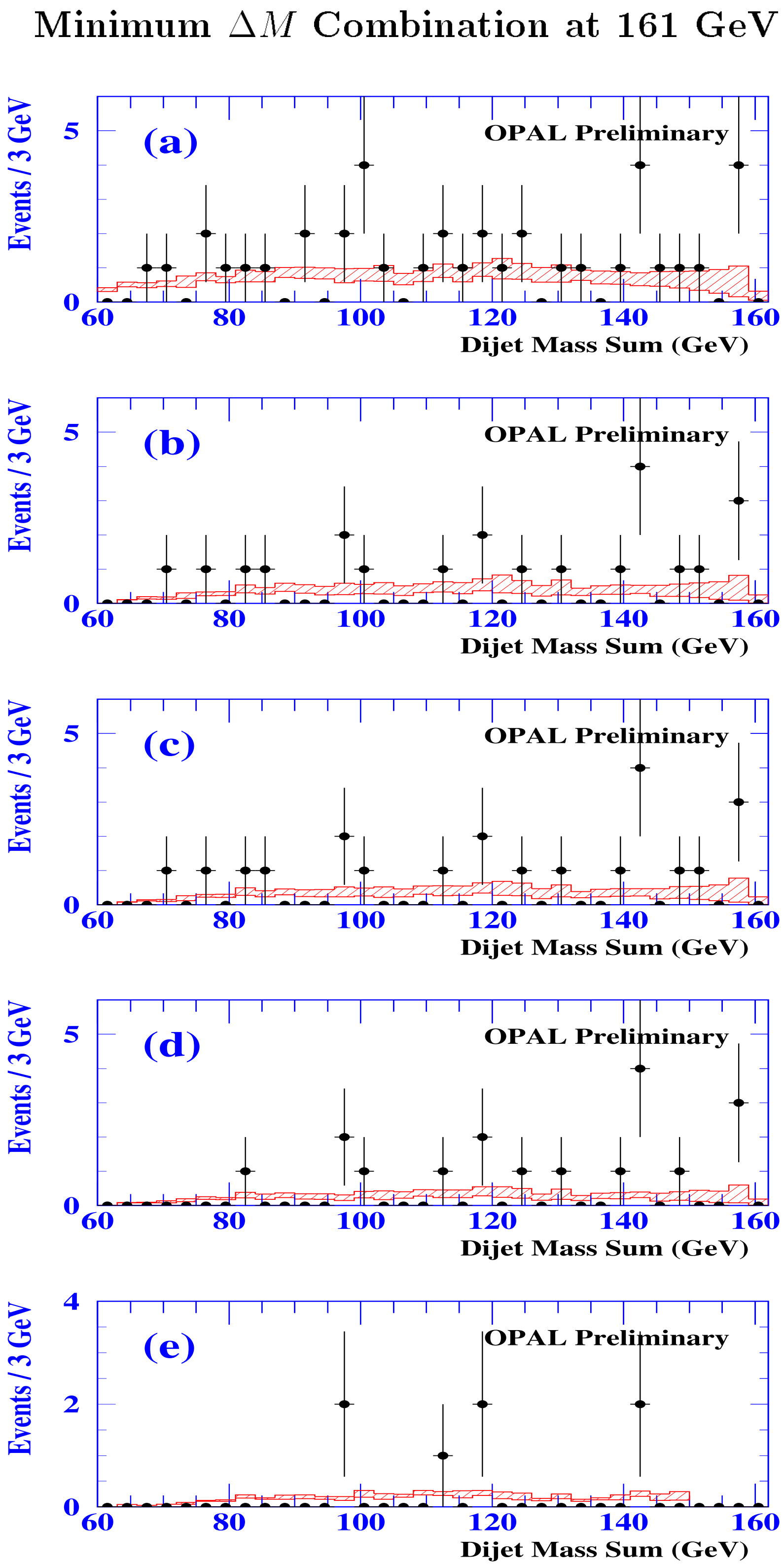

Figure 2: 161 GeV: The dijet mass sum for the combination with the smallest ΔM at different stages of the selection. Plots (a)–(e) show the distribution after cuts (6)–(10) respectively. Data are shown by points and Standard Model backgrounds by the histogram. The hatched component of the background histogram denotes four-fermion processes, while the unhatched component denotes $Z^0/\gamma^* \to q\overline{q}$.

Minimum ΔM Combination at 172 GeV

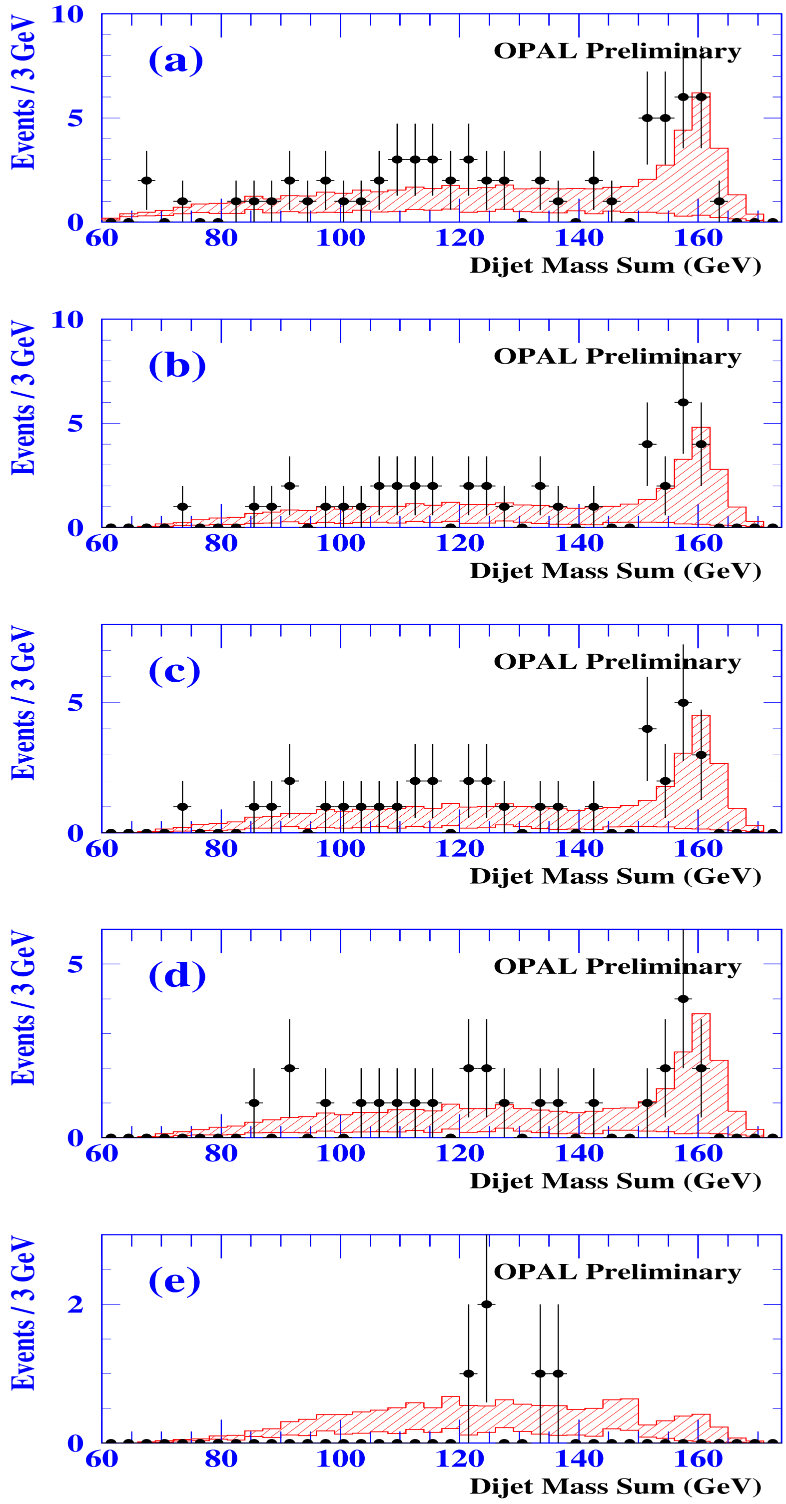

Figure 3: 172 GeV: The dijet mass sum for the combination with the smallest ΔM at different stages of the selection. Plots (a)–(e) show the distribution after cuts (6)–(10) respectively. Data are shown by points and Standard Model backgrounds by the histogram. The hatched component of the background histogram denotes four-fermion processes, while the unhatched component denotes $Z^0/\gamma^* \to q\overline{q}$.

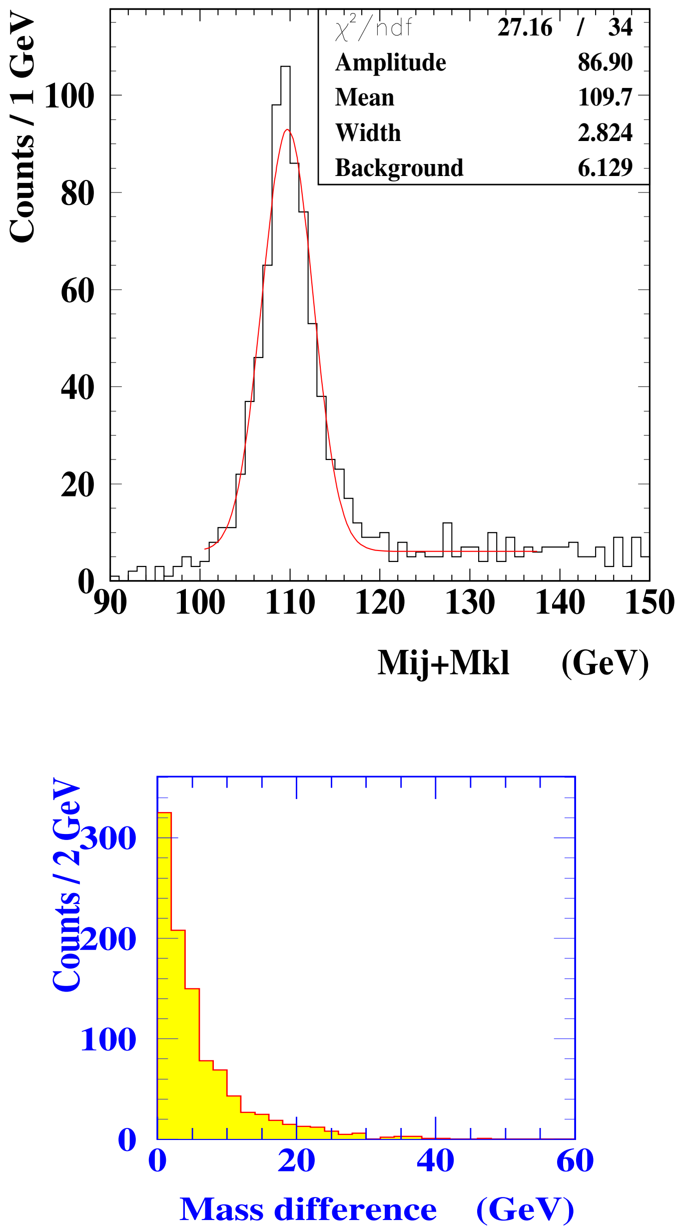

Figure 4: Top figure: Sum of the masses after cut (9), for a model signal with $m_h = m_A =$ 55 GeV, at $\sqrt{s} = 161$ GeV. The histogram is fitted with a Gaussian resolution function with a constant background. Parameters of the fit are shown in the plot. Bottom figure: Dijet pair mass differences reconstructed for the hA reference Monte Carlo, after cut (9). The jet pairing combination with minimum ΔM has been used for the plot.

Loose Selections at All Energies / no W-Pair Veto

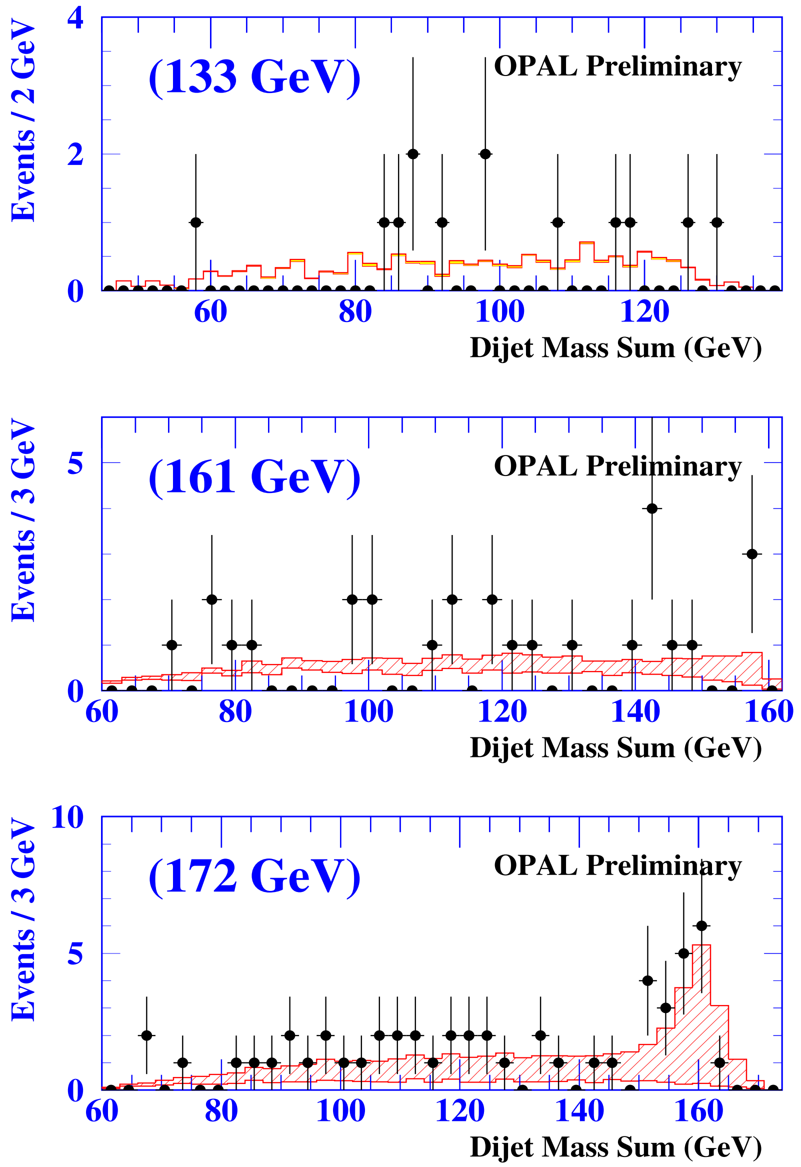

Figure 5: The dijet mass sum for the combination with the smallest ΔM after loosening selection cuts (7), (8), and (9) by 20%, separately for the three data samples. No W-pair veto has been applied. Data are shown by points and Standard Model backgrounds by the histogram. The hatched component of the background histogram denotes four-fermion processes, while the unhatched component denotes $Z^0/\gamma^* \rightarrow q\overline{q}$.

Additional Jet-Pair Combinations at 133 GeV

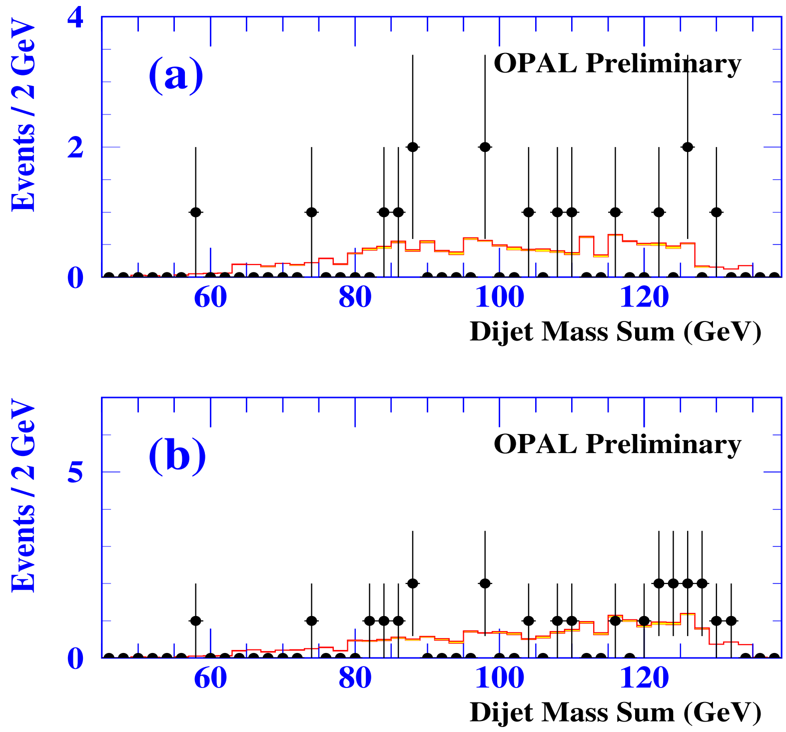

Figure 6: The dijet mass sum of selected events in the 133 GeV sample accumulating additional jet-pair combinations. Plot (a) contains entries from the combinations with the smallest and intermediate ΔM, and plot (b) contains entries from all three combinations. Data are shown by points and Standard Model backgrounds by the histogram. The hatched component of the background histogram denotes four-fermion processes, while the unhatched component denotes $Z^0/\gamma^* \rightarrow q\overline{q}$.

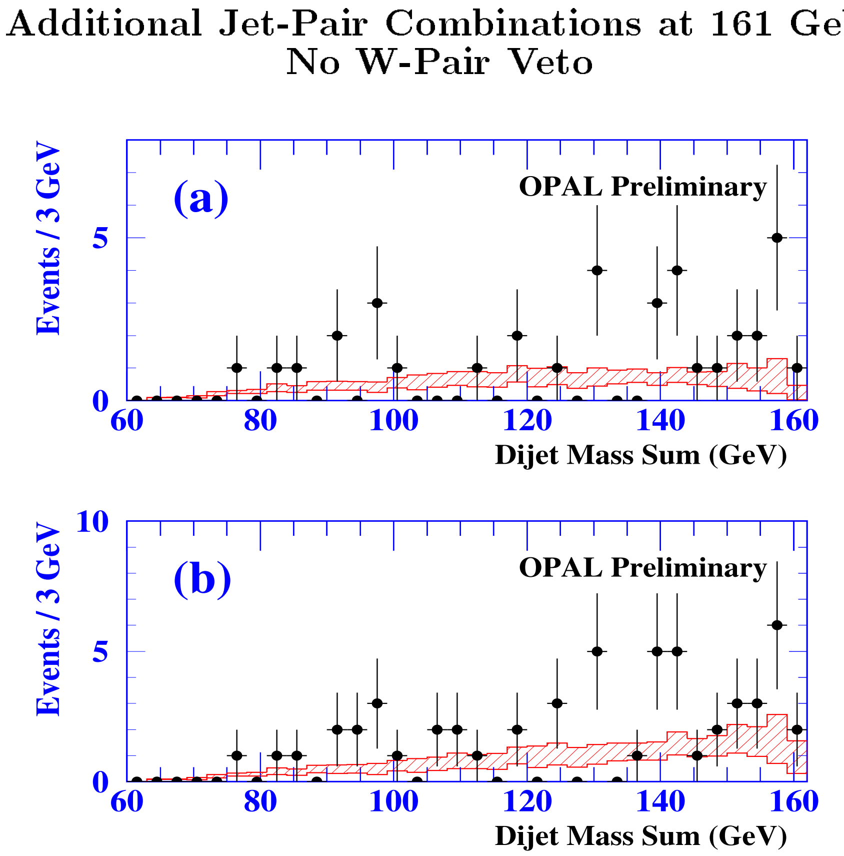

Figure 7: The dijet mass sum of selected events in the 161 GeV sample accumulating additional jet-pair combinations. Plot (a) contains entries from the combinations with the smallest and intermediate ΔM, and plot (b) contains entries from all three combinations. No W-pair veto has been applied. Data are shown by points and Standard Model backgrounds by the histogram. The hatched component of the background histogram denotes four-fermion processes, while the unhatched component denotes $Z^0/\gamma^* \rightarrow q\overline{q}$.

Additional Jet-Pair Combinations at 161 GeV
With W-Pair Veto

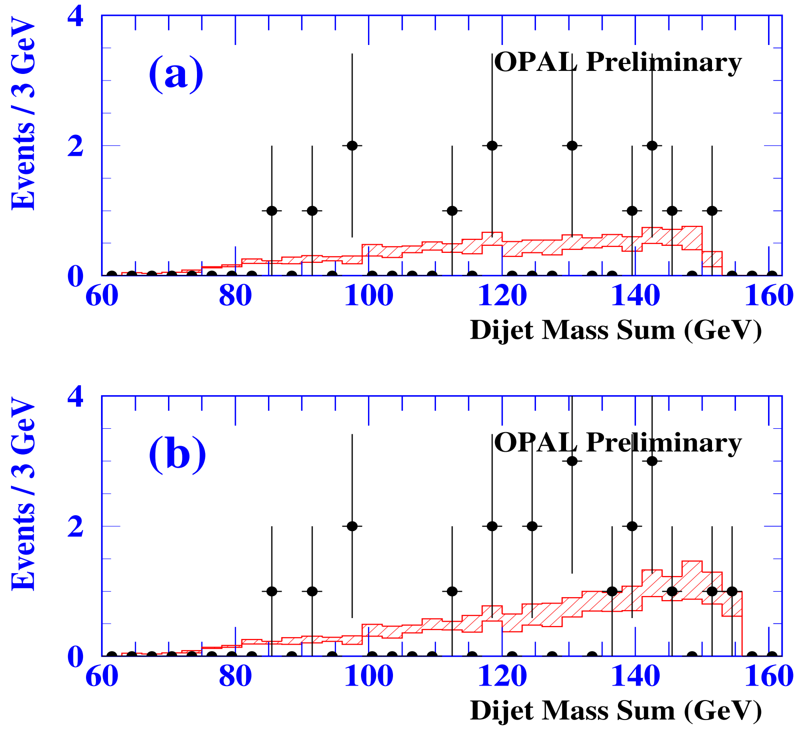

Figure 8: The dijet mass sum of selected events in the 161 GeV sample accumulating additional jet-pair combinations. Plot (a) contains entries from the combinations with the smallest and intermediate ΔM, and plot (b) contains entries from all three combinations. The W-pair veto has been applied in both plots. Data are shown by points and Standard Model backgrounds by the histogram. The hatched component of the background histogram denotes four-fermion processes, while the unhatched component denotes $Z^0/\gamma^* \rightarrow q\overline{q}$.

Additional Jet-Pair Combinations at 172 GeV
No W-Pair Veto

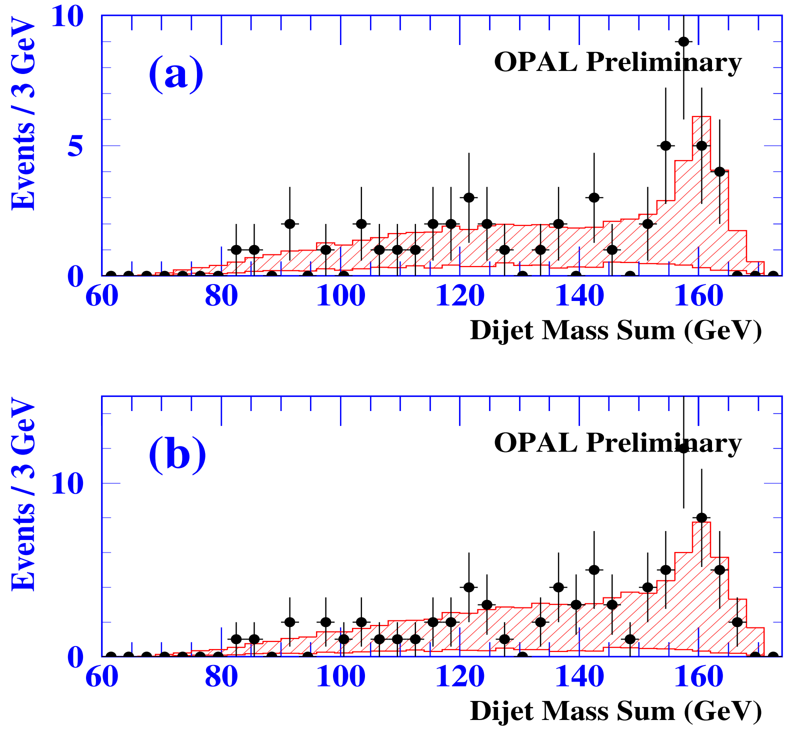

Figure 9: The dijet mass sum of selected events in the 172 GeV sample accumulating additional jet-pair combinations. Plot (a) contains entries from the combinations with the smallest and intermediate ΔM, and plot (b) contains entries from all three combinations. No W-pair veto has been applied. Data are shown by points and Standard Model backgrounds by the histogram. The hatched component of the background histogram denotes four-fermion processes, while the unhatched component denotes $Z^0/\gamma^* \to q\overline{q}$.

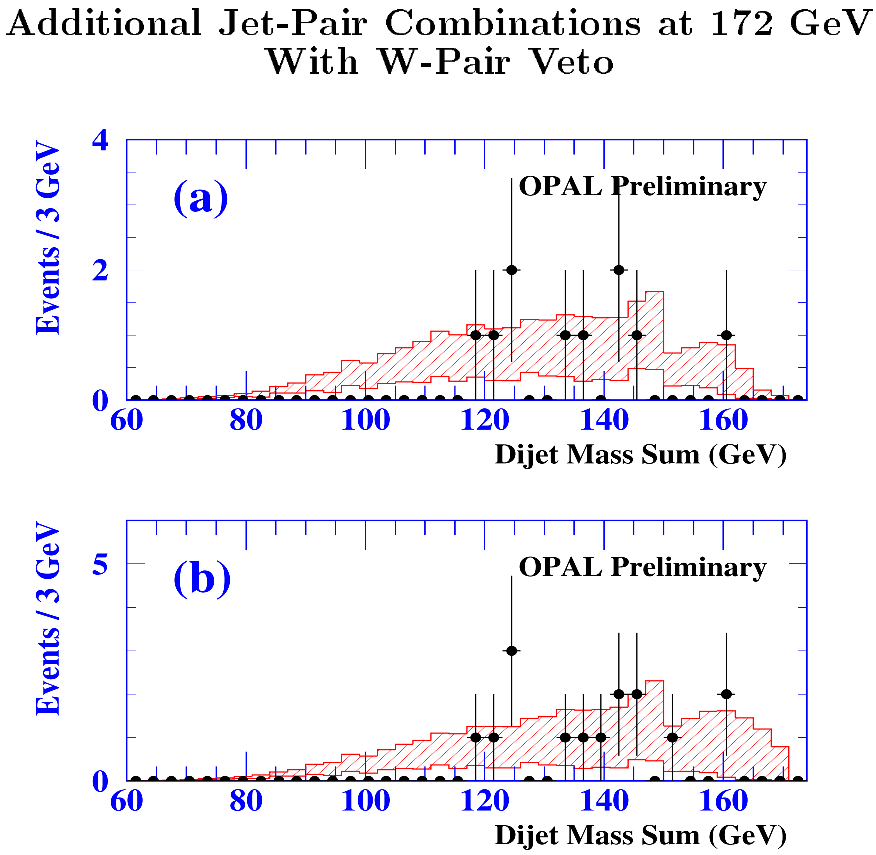

Figure 10: The dijet mass sum of selected events in the 172 GeV sample accumulating additional jet-pair combinations. Plot (a) contains entries from the combinations with the smallest and intermediate ΔM, and plot (b) contains entries from all three combinations. The W-pair veto has been applied in both plots. Data are shown by points and Standard Model backgrounds by the histogram. The hatched component of the background histogram denotes four-fermion processes, while the unhatched component denotes $Z^0/\gamma^* \rightarrow q\overline{q}$.

Combinations of All Energies / No W-Pair Veto

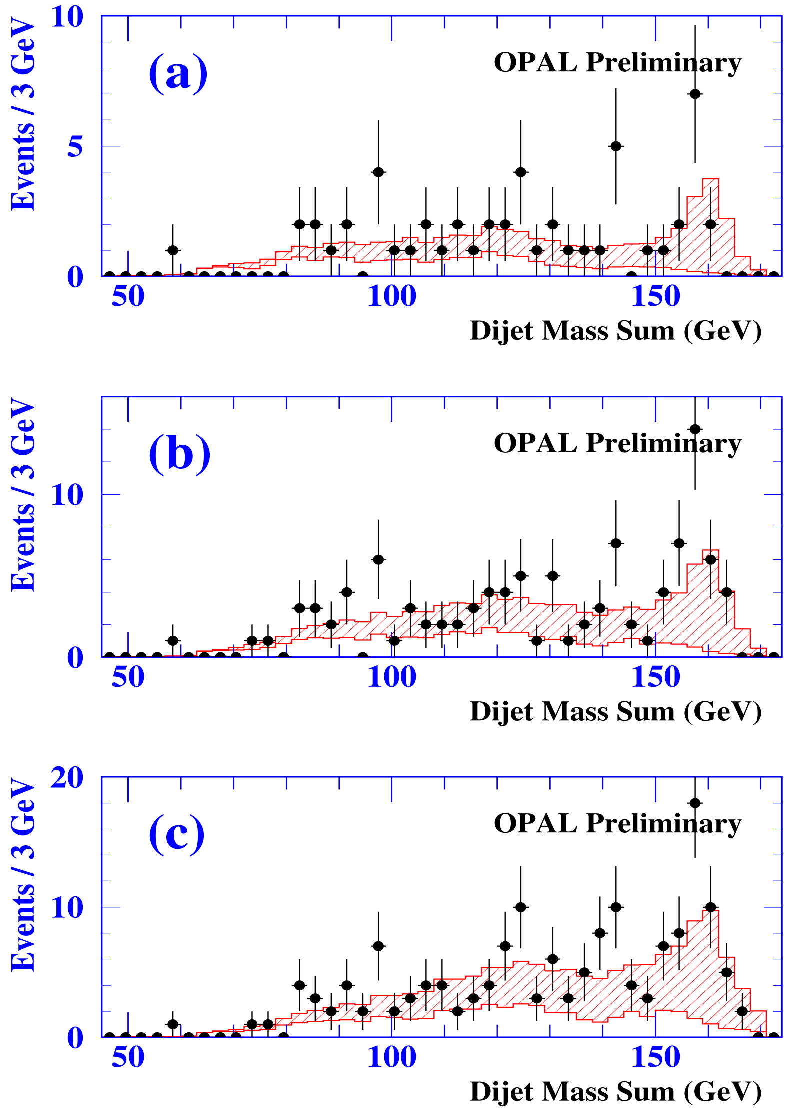

Figure 11: Distribution of the dijet mass sum for data combined from all three data samples after cut (9). The W-pair veto has not been applied. Plot (a) shows the distribution for the combination with the smallest ΔM, plot (b) accumulates the contributions from combinations for the smallest and the intermediate ΔM, and plot (c) contains contributions from all three combinations. Data are shown by points and Standard Model backgrounds by the histogram. The hatched component of the background histogram denotes four-fermion processes, while the unhatched component denotes $Z^0/\gamma^* \to q\overline{q}$.

Combinations of All Energies / W-Pair Veto

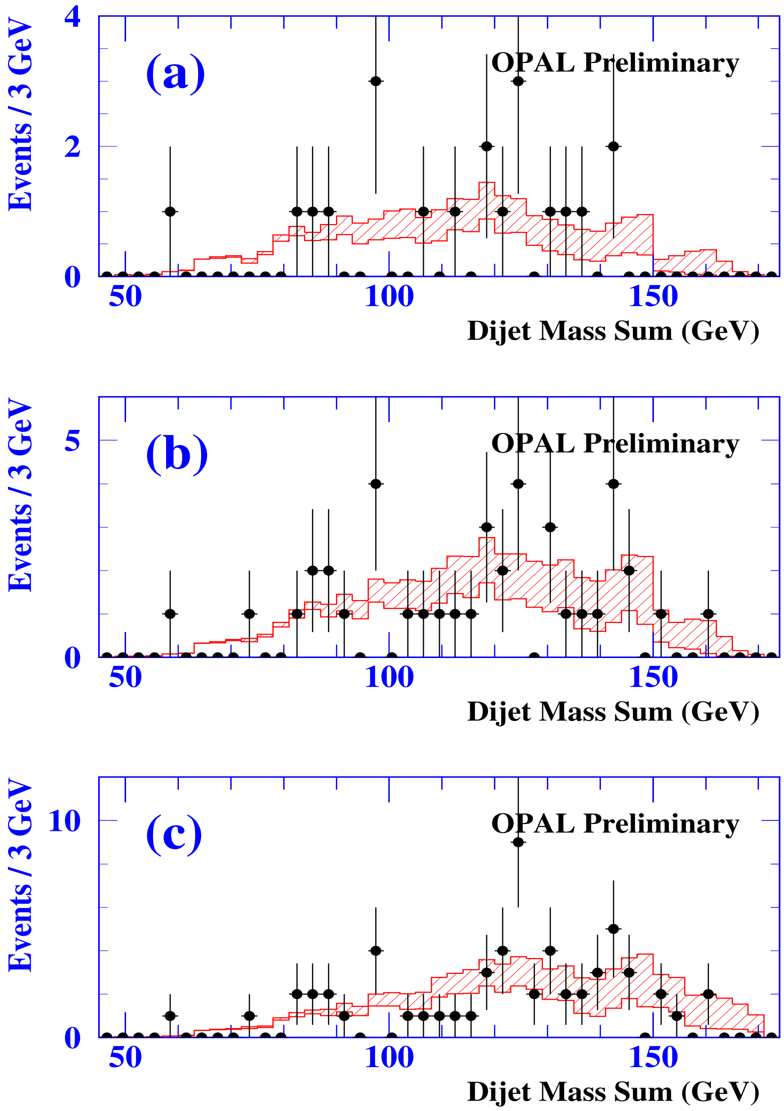

Figure 12: Distribution of the dijet mass sum for data combined from all three data samples after cut (9). The W-pair veto has been applied to the 161 and 172 GeV data samples. Plot (a) shows the distribution for the combination with the smallest ΔM, plot (b) accumulates the contributions from combinations for the smallest and the intermediate ΔM, and plot (c) contains contributions from all three combinations. Data are shown by points and Standard Model backgrounds by the histogram. The hatched component of the background histogram denotes four-fermion processes, while the unhatched component denotes $Z^0/\gamma^* \rightarrow q\overline{q}$.

Sliding mass window for all energies / no W-pair veto

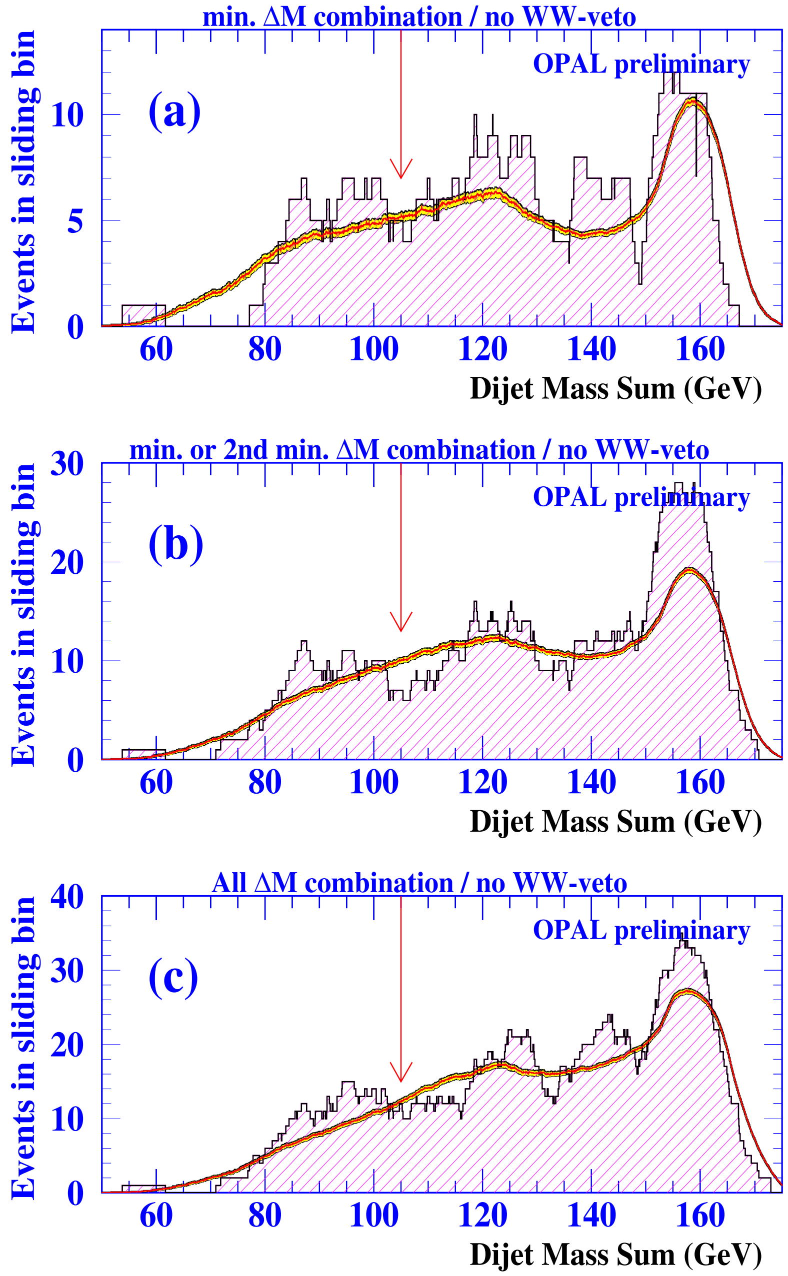

Figure 13: Results of the sliding mass window scan for selected events after cut (9) (all selection requirements applied except the W-pair veto), accumulating data taken at the three centre-of-mass energies. The hatched histogram shows the total number of events observed in the data in mass windows of ± 4.0, 5.6, and 6.0 GeV for the 133, 161, and 172 GeV samples, respectively, centered on the abscissa value. The solid line represents the Standard Model background expectation, and the width of the line corresponds to the Monte Carlo statistical error. Plot (a) shows data for the combination with the smallest ΔM, plot (b) the smallest and intermediate ΔM, and plot (c) all three combinations. The arrows are drawn at 105 GeV.

Sliding mass window for all energies / with W-pair veto

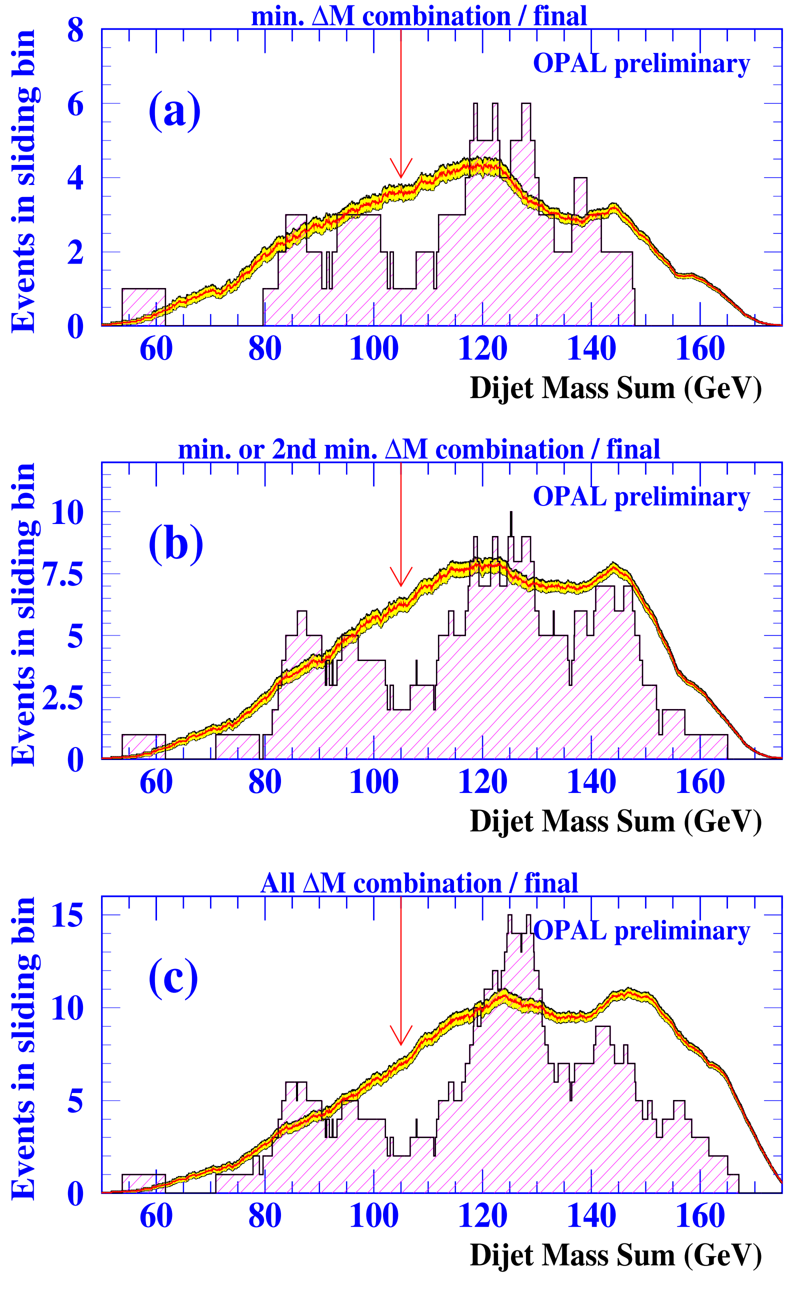

Figure 14: Results of the sliding mass window scan for events passing all selection criteria in all three data samples. The W-pair veto has been applied in the 161 and 172 GeV data samples. The hatched histogram shows the total number of events observed in the data in mass windows of ± 4.0, 5.6, and 6.0 GeV for the 133, 161, and 172 GeV samples, respectively, centered on the abscissa value. The solid line represents the Standard Model background expectation, and the width of the line corresponds to the Monte Carlo statistical error. Plot (a) shows data for the combination with the smallest ΔM, plot (b) the smallest and intermediate ΔM, and plot (c) all three combinations. The arrows are drawn at 105 GeV.